[DOI: 10.1063/1.2217440]

Direct observation and reactions of Cl_3 radical

Shinichi Enami, Takashi Yamanaka, Satoshi Hashimoto, and Masahiro Kawasaki
Department of Molecular Engineering, Kyoto University, Kyoto 615-8510, Japan

Simone Aloisio
California State University, Channel Islands, One University Drive, California 93010

Hiroto Tachikawa
Department of Materials Chemistry, Graduate School of Engineering, Hokkaido University, Sapporo 060-8628, Japan

The broad absorption of Cl_3 radical was observed between 1150 and 1350 nm using cavity ring-down spectroscopy at 213–265 K and 50–200 Torr with He, N_2, Ar, or SF_6 diluents. The absorption intensity of Cl_3 increased at lower temperature and higher pressure. SF_6 was the most efficient diluent gas. The temperature dependent equilibrium constants for Cl_3 formation from $Cl+Cl_2$ were theoretically calculated at the MP4SDQ/6-311+G(*d*) level. Observed decay time profiles of Cl_3 and the pressure dependence of Cl_3 formation are explained by the equilibrium reaction and a decay reaction of $Cl+ Cl_3$.

INTRODUCTION

Trihalogens have been proposed to explain halogen atom recombination reactions.[1–4] Crossbeam scattering experiments by Lee and co-workers[5–8] suggested the existence of bound trihalogens in the gas phase reactions. Fluorine containing trihalogens were observed and characterized in rare gas matrices using infrared (IR) absorption and Raman spectroscopy.[9–13]

Hutton and Wright[3] proposed a formation mechanism of trichloride radical Cl_3 from Cl atom recombination in the presence of Cl_2,

$$Cl + Cl_2 + M \rightarrow Cl_3 + M, \quad (1a)$$

$$Cl + Cl_2 + M \leftarrow Cl_3 + M, \quad (1b)$$

$$Cl_3 + Cl \rightarrow 2\ Cl_2. \quad (2)$$

Existence of Cl_3 was reported experimentally[2–4,14–16] and theoretically.[17–23] Emission spectra attributable to Cl_3 were observed by Kawasaki *et al.*[14] and Wright *et al.*[15] These data were in reasonable agreement with each other. An IR spectrum of Cl_3 in a Kr matrix was reported by Nelson and Pimentel.[24] However, Wight *et al.*[25] indicated that the species they observed was not Cl_3 radical but Cl^-_3 anion.

An *ab initio* study by Kaledin *et al.*[23] showed that the structure in the global minimum of the Cl_3 radical is linear $^2\Pi_{3/2}$ with a bond dissociation energy $D_e(Cl_2–Cl)$ of 280 cm^{-1}. Kaledin *et al.* [23] reported that the energies and transition moments of the low-lying excited states are not consistent with the experimental electronic ultraviolet and visible

spectra that have been assigned to Cl_3. They also suggested that the low-lying doublet excited state is a bound symmetric $1\ ^2\Pi_g$ state, and its potential minimum lies about 8700 cm^{-1} above the van der Waals minimum. They concluded that the $A-X$ transition is fully allowed.

The present study is the first report on the Cl_3 absorption in the near-IR region. Time-resolved cavity ring-down spectroscopy[26–29] (CRDS) was used to search for the electronic transition of Cl_3. We obtained theoretically the equilibrium constants for reactions (1a) and (1b) and experimentally the rate constants for reactions (1a), (1b), and (2).

EXPERIMENT

The CRDS apparatus used in the present study has been described in detail elsewhere.[30,31] Cl atoms were generated by photodisocciation of Cl_2 at 355 nm [Nd^{3+} :YAG (yttrium aluminum garnet) laser, Spectra Physics, GCR-250]. A typical laser intensity was 80±5 mJ $pulse^{-1}$. The output from an optical parametric oscillation laser (Spectra-Physics, MOPOSL, 0.2 cm^{-1} spectral resolution) was used to obtain the desired probe wavelengths in the near-IR region. A dye laser (Lambda Physik ScanMate pumped by the second harmonic output from a Nd^{3+} :YAG laser, Quantel, Brilliant *β)* with coumarin dye (480 nm or 440 nm) was also used to probe Cl_3 in the visible region. Cavity ring-down mirrors (II-VI or Research Electro Optics, 7.8 mm diameter and 1 m curvature) had a specified maximum reflectivity of >0.999 and were mounted 1.04 m apart. Light leaking from the end mirror was detected by a photodiode (Thorlabs, PDA255) or a photomultiplier tube (Hamamatsu Photonics, R212UH) through a proper cutoff filter. The ring-down signal of the light intensity was sampled by a digitizing oscilloscope (Tektronix, TDS-714L, 500 MHz, 8-bit resolution) and recorded in a personal computer (PC).

The decay of the leaked light intensity from the end mirror is represented by Eq. (3),

$$I(t) = I_0 \exp(-t/\tau) = I_0 \exp(-t/\tau_0 - \sigma n c L_R t/L), \qquad (3)$$

where I_0 and $I(t)$ are the light intensities at times 0 and t, respectively. τ_0 is the cavity ring-down time without photolysis laser light (about 1.5 μs at 1300 nm and 1.5 μs at 440 nm), L_R the length of the reaction region (0.40±0.01 m), L the cavity length (1.04 m), τ the measured cavity ring-down time with photolysis laser light, and c the velocity of light. n and σ are the concentration and absorption cross section of the species of interest, respectively. Each ring-down trace was digitized with a time resolution of 20 ns. The digitized traces were transferred to the PC and averaged over 32 or 64 runs to calculate the ring-down rate τ^{-1}. The validity of using cavity ring-down spectroscopy for kinetic studies derives from the fact that the lifetimes of the products generated by photolysis are much longer than the associated cavity ring-down times.[29]

The reaction cell consisted of a Pyrex glass tube (21 mm inner diameter), which was evacuated by a combination of an oil rotary pump and a mechanical booster pump. The temperature of the gas flow region was controlled over the range 213–298 K by circulation of ethanol with a cooling circulator (Thomas, TRL 70 SLP). The difference between the temperature of the sample gas at the entrance and exit of the flow region was <1 K. Since the reaction region was located in the center 40 cm of the glass reactor, the temperature was uniform in the interaction region. The pressure in the cell was monitored by an absolute pressure gauge (Baratron, 622A). Gas flows were regulated by mass flow

controllers (STEC, SEC-E40). A slow flow of N2 diluent gas was introduced at the ends of the ring-down cavity, close to the mirrors, in order to minimize deterioration caused by exposure to the reactants and the products in the cell. The total flow rate was kept constant at 2.0×10^3 cm^3 min^{-1} (STP). Cl_2 gas was supplied from prepared glass bulbs. The concentrations of these gases were calculated by the flow rates of each mass flow controller and the reactant concentration in the gas bulbs. Typical concentrations of Cl_2 were (1–10) x 10^{16} molecule cm^{-3}. Photochemically produced Cl($^2P_{1/2}$) atoms were rapidly relaxed to Cl($^2P_{3/2}$) by collisions with N_2 under our pressure conditions.[32,33] To estimate the initial concentration of the Cl atoms, $[Cl]_0$, the loss of O_3 and the production of ClO were independently measured at 266 nm using $Cl_2/O_3/O_2$ mixtures with photolysis of Cl_2 at 355 nm.[31]

All reagents were obtained from commercial sources, Cl_2 (>99.999%, Japan Air Liquid Co.), N_2 (>99.999%, Teisan Co.), He (>99.998%, Teisan Co.), Ar (>99.998%, Teisan Co.), and SF_6 (>99.999%, Kanto Denka Kougyou Co.)

EXPERIMENTAL RESULTS

Absorption spectra

After 355 nm irradiation of a Cl_2/N_2 mixture, unstructured transient absorption appeared in the near-IR region of 1150–1350 nm at 213 K. Figure 1 shows the absorption spectrum at 0.1 ms after UV irradiation of the mixture of 4.5×10^{16} molecule cm^{-3} of Cl_2 with 100 Torr total pressure of N_2 diluent at 355 nm. The broad base line was measured without 355 nm irradiation. Its contribution to the spectra was subtracted from the raw absorption spectrum. No absorption appeared in the near-IR region by photoirradiation at 266 or 532 nm. To check for heterogeneous reactions or impurities, a variety of parts of the experimental setup, e.g., the reaction cell, glass bulbs, mass flow controllers, connectors, and o rings, were swapped for identical ones. We do not think that these were responsible for the absorption observed.

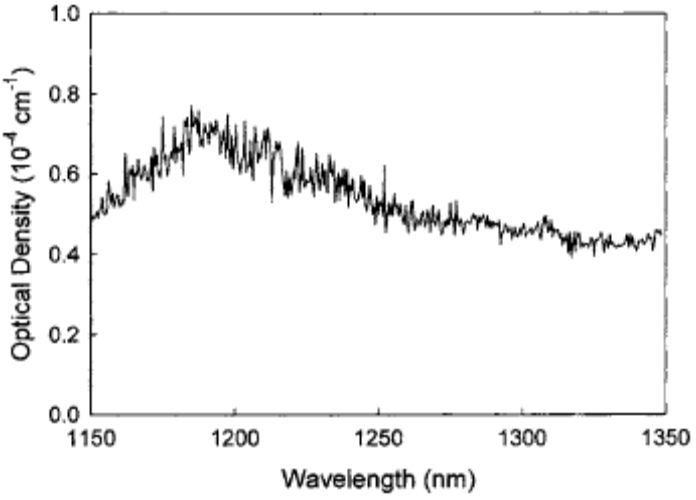

FIG. 1. Absorption spectrum obtained from the 355 nm irradiation of Cl_2 at 213 K, 100 Torr total pressure of N_2 diluent, and 0.1 ms after photolysis.

We also checked the possibility of formation of aerosols from photoirradiation of chlorine gas. A mixture of 4.5×10^{16} molecule cm^{-3} of Cl_2 and 100 Torr of N_2 was introduced into the reaction cell in batch system and photoirradiated at 355 nm (120 mJ $pulse^{-1}$, 10Hz) for 15–30 s at 213 K. We could not find any difference between before and after photoirradiation in the ring-down signal. These results indicate that aerosols which survive for longer than seconds were not formed in our experimental conditions. Considering all of these results, we conclude that the absorption appearing in the Cl_2/N_2 mixture with 355 nm irradiation is attributed to the reaction product Cl_3.

We also attempted to detect transient photoabsorption at 430–450 and 460–500 nm. Chlorine concentration [Cl_2] was varied in the range from 9.0×10^{15} to 1.1×10^{17} molecule cm^{-3} for these experiments in 100 Torr total pressure of N_2 diluent at 213 K. Unfortunately, we could not obtain the quantitative experimental evidence of the absorption of Cl_3 at these wavelength regions because of the significant absorption of Cl_2 itself.

Kinetic study

Figure 2 shows a typical decay time profile of the Cl_3 absorption intensity at 1250 nm, [Cl_2]=1.0×10^{17} molecule cm^{-3}, and 100 Torr N_2 diluent. As shown in Fig. 3, the absorption intensity at 1250 nm and 0.1 ms after UV irradiation increased linearly with the photolysis laser intensity at 355 nm. Figure 4 shows the absorption intensity of Cl_3 as a function of Cl_2 concentration at 0.1 ms delay. It is apparent that [Cl_2] dependency is nonlinear. This behavior indicates that the production rate of Cl_3 is proportional to both [Cl] and [Cl_2], since formation of Cl_3 is an equilibrium reaction. These results indicate that the observed absorption is not attributable to the Cl*M* complex (*M*=N_2, Ar, and He) proposed by Baer *et al.* in high total pressure conditions (1–1000 bars).[34] Figure 5 shows the buffer pressure dependence of the absorption intensity of Cl_3 at 213 K with N_2 diluent at 0.1 ms delay. The concentration of Cl_2 was 9.1×10^{16} molecule cm^{-3}. Production of Cl_3 increased with total pressure. He, Ar, and SF_6 were also used as buffer gases to examine the third-body efficiency on the formation of Cl_3. The order of the third-body efficiency was $SF_6 > N_2 = Ar > He$ as shown in Table I. Figure 6 shows a negative temperature dependence of the absorption intensities of Cl_3 at 1160, 1200, and 1250 nm, which are normalized to the absorption intensity at 230 K, 100 Torr total pressure of N_2 diluent, 0.1 ms delay, and [Cl_2]=9.6×10^{16} molecule cm^{-3}.

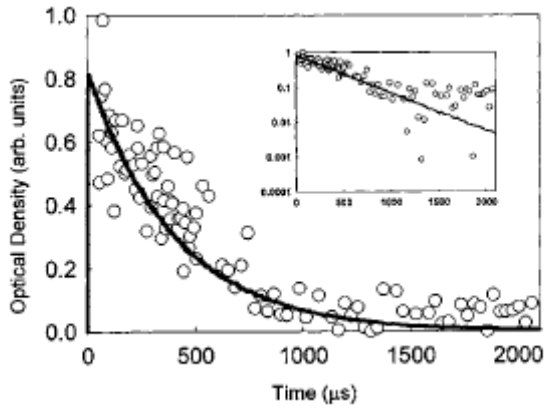

FIG. 2. A typical decay time profile of the absorption intensity of Cl_3 at 1250 nm at 213 K and 100 Torr total pressure of N_2 diluent. The inset shows the semilogarithm plots. $[Cl_2]=1.0 \times 10^{17}$ molecule cm^{-3}. The solid line is a simulation result. See text for details.

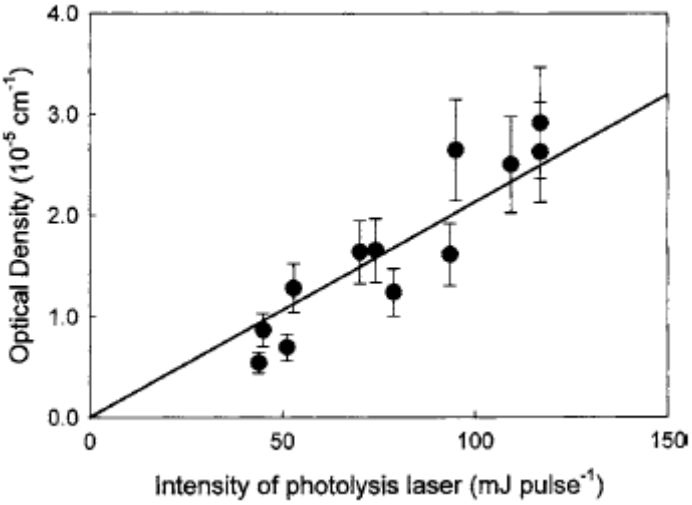

FIG. 3. Photolysis laser intensity dependence of the absorption of Cl_3 at 213 K and 100 Torr total pressure of N_2 diluent. $[Cl_2]=1.9 \times 10^{16}$ molecule cm^{-3} and 0.1 ms after photolysis.

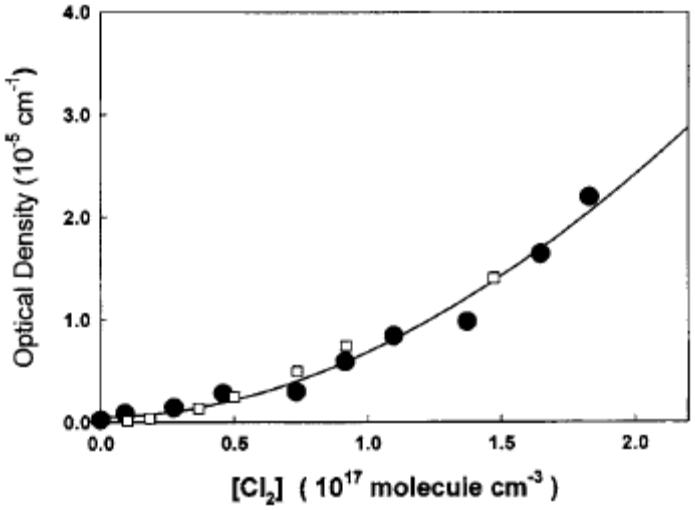

FIG. 4. Absorption intensities of Cl_3 at 1250 nm and 0.3 ms after photolysis as a function of [Cl_2] at 213 K and 100 Torr total pressure of N_2 diluent. The solid curve is a best fit of Eq. (6). Squares are the results of simulation for reactions (1a), (1b), and (2). See text for details.

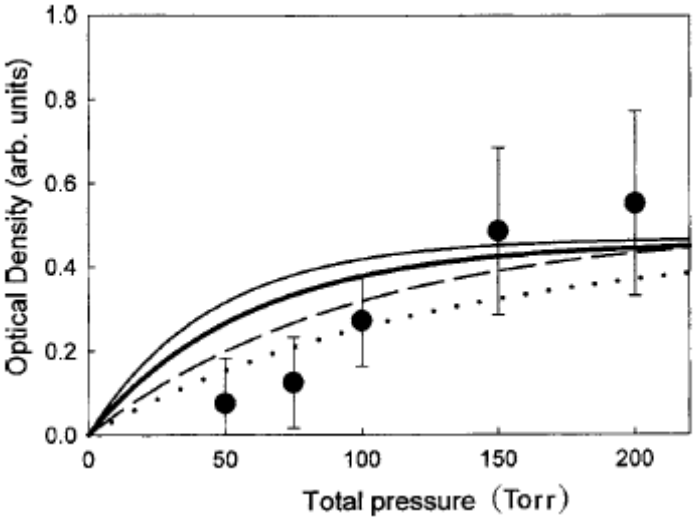

FIG. 5. Pressure effect of N_2 on formation of Cl_3 at 213 K and 0.1 ms after photolysis. Concentration of Cl_2 is 9.1 x 10^{16} molecule cm^{-3}. The solid curves are fitting results with $k_{(2)}$=4.0 x 10^{-10} cm^3 $molecule^{-1}$ s^{-1} (thick) and 2.5 x 10^{-10} cm^3 $molecule^{-1}$ s^{-1} (thin) for the linear structure. $k_{(2)}$=4.0 x 10^{-10} cm^3 $molecule^{-1}$ s^{-1} (dot) and 2.5 x 10^{-10} cm^3 $molecule^{-1}$ s^{-1} (dash) for the bent structure. See text for details of simulation.

TABLE I. Relative buffer gas effects on the absorption intensity of Cl_3 at 1250 nm and T=213 K.

Buffer gas	Relative absorption of Cl_3 at 50 Torr (normalized to N_2)
He	0.7±0.3[a]
N_2	1.0
Ar	0.8±0.3
SF_6	1.8±0.7

[a]Total pressure of He was 200 Torr.

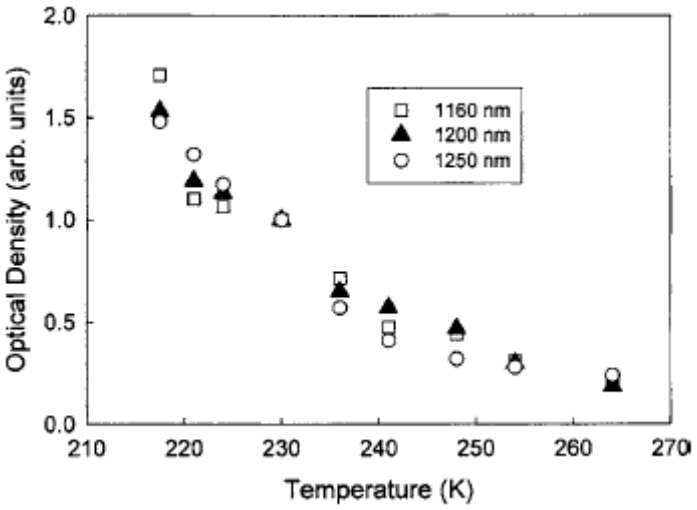

FIG. 6. Temperature dependence of the relative absorption intensities at 1160, 1200, and 1250 nm, normalized to the absorption intensity at 230 K. 100 Torr total pressure of N_2 diluent. $[Cl_2]=9.6 \times 10^{16}$ molecule cm^{-3}.

Reaction of Cl_3 with CH_4

We tried to check whether the time profiles of the absorption intensity of Cl_3 will change or not when we added CH_4 to the reaction cell,

$$Cl_3 + CH_4 \rightarrow \text{products.} \qquad (4)$$

No decay change of Cl_3 was observed with $(2.0–5.3) \times 10^{15}$ molecule cm^{-3} of CH_4 at 219 K and 100 Torr total pressure of N_2 diluent as shown in Fig. 7. As described below, the decay is mostly governed by the diffusion rate of Cl_3 from the detection region and the equilibrium rates. Since there was no change in the Cl_3 decay, the reaction rate of Cl_3 with CH_4 is much smaller than the diffusion rate.

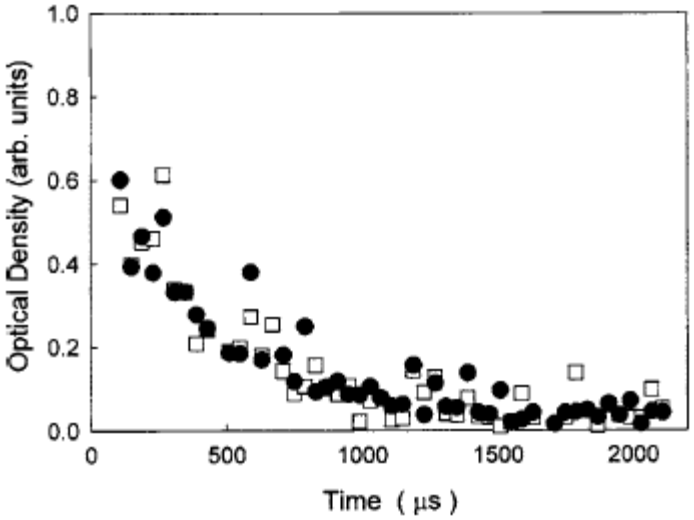

FIG. 7. Decay profiles of Cl_3 with 3.3 x 10^{15} molecule cm^{-3} of CH_4 (circle) or without CH_4 (square) at 219 K and 100 Torr total pressure of N_2 diluent. The concentration of Cl_2 was 5.5 x 10^{16} molecule cm^{-3}.

Theoretical calculations

All *ab initio* calculations were carried out using the GAUSSIAN 03 program package.[35] The structures and harmonic vibrational frequencies of Cl_3 and Cl_2 were calculated at the MP4SDQ/6-311+G(*d*) level. Two structural forms of the Cl_3 radical, linear and bent forms, are obtained by the geometry optimization. The optimized parameters are given in Table II. The structural parameters of the linear form of Cl_3 radical are calculated to be r_1=2.0374 Å, r_2=3.5988 Å, and θ =180.0°, where r_1 and r_2 indicate short and long Cl–Cl bond lengths of the Cl_3 radical, respectively, and θ means the angle of Cl–Cl–Cl. In the case of the bent form, the optimized parameters are r_1=2.0365 Å, r_2=3.4962 Å, and θ =94.7°. In both forms, one of the Cl–Cl distances of the Cl_3 radical (r_2) is significantly longer than the other (r_1), indicating that the Cl_3 radicals exist as a van der Waals complexes composed of a Cl_2 molecule and Cl atom, as predicted by Kaledin *et al.*[23] Harmonic vibrational frequencies of the Cl_3 radicals are given in Table III. The frequencies are calculated to be 528, 41, and 25 cm^{-1} for the linear form and 530, 50, and 22 cm^{-1} for the bent form. The zero-point energies (ZPEs) are 0.89 kcal/mol for the linear form and 0.86 kcal/mol for the bent form. All vibrational frequencies show positive values, meaning that the optimized structures of the Cl_3 radicals are located in local minima. The binding energy of the Cl atom to the Cl_2 molecule is calculated to be
350 cm^{-1} (without ZPE correction) and 300 cm^{-1} (including ZPE correction) for the linear form and 370 cm^{-1} (without ZPE correction) and 344 cm^{-1} (including ZPE correction) for the bent form.

The equilibrium constant of the Cl_3 formation reaction [(1a) and (1b)] is estimated by

$$K = \frac{Q(\mathrm{Cl_3})}{Q(\mathrm{Cl})Q(\mathrm{Cl_2})} \exp\left(-\frac{\Delta U}{k_B T}\right), \qquad (5)$$

where Q's are the molecular partition functions and ΔU is the formation energy of Cl_3 expressed by Eq. (5). The harmonic approximation is assumed in the calculation of vibrational frequencies. The total partition function Q is expressed on the product of vibrational, rotational, translational, and electronic partition functions. To estimate the rotational partition function, classical behavior for the rotation of Cl_3 is assumed. The equilibrium constants at 213 K for the linear form are calculated to be 2.49×10^{-20} cm^3 $molecule^{-1}$ at the MP4SDQ/6-311+G(d) level. The temperature dependence of K is given in Fig. 8. The equilibrium constant decreases with increasing temperature; at 298 K, K=1.38×10^{-20} cm^3 $molecule^{-1}$. The equilibrium constant for the bent form is calculated to be K=1.12×10^{-19} $cm^3 molecule^{-1}$ at 213 K, which is about four times larger than that of the linear form. Similar calculations were carried out at the MP2/6-311+ +G(d, p) level. The equilibrium constants for the linear and bent forms are calculated to be K=2.65×10^{-20} and 1.13×10^{-19} cm^3 $molecule^{-1}$ at 213 K. Furthermore, the equilibrium constant at 213 K is calculated using anharmonic frequencies of the Cl_3 radical obtained at the MP2/6-311+ +G(d, p) level. The values for the linear and bent forms are calculated to be K(anharmonic)=2.70×10^{-20} and 2.15×10^{-19} cm^3 $molecule^{-1}$ at 213 K, respectively. Contribution of anharmonic effect increases the equilibrium constants for the bent form.

Hutton and Wright experimentally determined the lower limit value of the equilibrium constant, K>2.0 x 10−22 cm^3 $molecule^{-1}$.[3] Our present data are consistent with that of Hutton and Wright. Kaledin *et al.* predicted that the equilibrium constant at 295 K is 6.7 x 10−23 cm^3 $molecule^{-1}$, which is significantly smaller than the experimental value. The difference may be caused by underestimation of $-\Delta U$ in their calculation because the Cl–Cl bond length of the Cl_3 radical was fixed in the geometry optimization. If we used the K value reported by Kaledin *et al.*,[23] the concentration of Cl_3 should become too low to be detected experimentally.

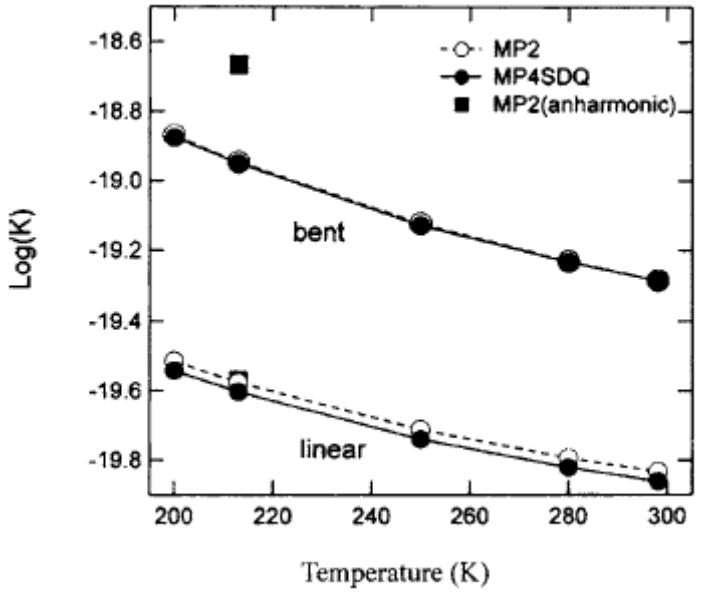

FIG. 8. Temperature dependence of the equilibrium constants (K in cm^3 $molecule^{-1}$) calculated at the MP4SDQ/6-311+G(d) and MP2/6-311 +G(d) levels of theory.

TABLE II. Optimized parameters of Cl_3 calculated at the MP4SDQ/6–311 +G(*d*) level. Bond lengths and angles are in angstroms and in degrees, respectively.

	MP4SDQ/6-311+G(*d*)		MR-SD-CI[a]	
	Linear	Bent	Linear	Bent
r_1	2.0374	2.0365	2.0638	2.0638
r_2	3.5988	3.4962	3.5720	3.4982
θ	180.0	94.7	180.0	95.8

[a]From Ref. [23].

TABLE III. Harmonic vibrational frequencies of Cl_3 (in cm^{-1}) and zeropoint energies (ZPEs in kcal/mol) calculated at the MP4SDQ/6-311+G(*d*) level.

Mode	Assignment	Cl_3 (linear)	Cl_3 (bent)
ν_1	Cl–Cl stretching	528[a]	530[a]
ν_2	Cl–Cl_2 stretching	41	50
ν_3	Bending	25[b]	22
Zero-point energy		0.89	0.86

[a]The Cl–Cl stretching mode of free Cl_2 is calculated to be 529.0 cm^{-1} (ZPE=0.76 kcal/mol).
[b]Doubly degenerated mode (π-bending mode).

DISCUSSION

Phototransition

Previous experimental observations of emission of Cl_3 were reported by two groups.[14,15] Kawasaki *et al.* reported the excitation spectrum of Cl_3 at 415–427 nm with the use of laser induced fluorescence (LIF).[14] Wright *et al.* also observed a broadband emission in the 370–440 nm regions at 400 Torr total pressure of N_2 diluent.[15] These results support the existence of Cl_3. The present results show a new band at 1150–1350 nm.

Kaledin *et al.* reported that the low-lying doublet excited state is a bound linear symmetric $1\,^2\Pi_g$ state (an excited state complex), and its potential minimum lies about 8700 cm^{-1} above the van der Waals minimum.[23] The vertical electronic transition point is a further 9000 cm^{-1} higher in energy than the potential minimum of the excited state complex. Namely, the vertical excitation energy of Cl_3 is calculated to be 17 700 cm^{-1} from the van der Waals minimum. However, the van der Waals complex has a wide Franck-Condon region due to its structural flexibility, including the bent structure. Furthermore, the energy level of the excited state complex is significantly low (8700 cm^{-1}), while the relaxation energy from the vertical point to the excited state complex is large (9000 cm^{-1}). Therefore, absorption spectrum of Cl_3 would appear in the energy

region 8700–17700 cm^{-1}. This excitation energy is consistent with that observed in the present experiment (7400–8710 cm^{-1}). Kaledin *et al.* also reported that the *A*-*X* transition is fully allowed. The absorption spectrum of Cl_3 observed in the present study could be assigned to be the *A*-*X* transition from the wide Franck-Condon region of the van der Waals complex.

Reaction mechanism of Cl_3 formation and decay

As shown in Fig. 6, Cl_3 formation has a negative temperature dependence. These results are similar to that of ClOO formation, which is considered as a weak van der Waals complex with the bond dissociation energy of 1640 cm^{-1}.[30]

Assuming only the equilibrium reactions (1a) and (1b), the following equation is obtained:

$$[Cl_3]_{eq} = K[Cl_2][Cl]_0/(1 + K[Cl_2]). \quad (6)$$

The solid curve in Fig. 4 is a best-fit curve for Eq. (6), which well approximates the concentration dependence of Cl_3 on $[Cl_2]$. However, the reaction of Cl_3 with Cl should be included to determine the concentration of Cl_3 correctly. The rate constants of reactions (1a) and (2) were obtained only from the decay time profiles of the absorption intensity of Cl_3 and the buffer pressure dependence of the absorption intensity of Cl_3 in chemical simulations that were performed using the IBM chemical kinetics simulator software package and the reactions listed in Table IV. Simulation conditions were as follows; $[Cl_2]=9.3 \times 10^{16}$ molecule cm^{-3}, $[Cl]_0=1.0 \times 10^{15}$ molecule cm^{-3}, photolysis laser intensity of 73 mJ $pulse^{-1}$, and 100 Torr total pressure of N_2 diluent at 213 K. $[Cl]_0$ was determined using the laser intensity and $[Cl_2]_0$. Using the theoretically obtained $K=2.7 \times 10^{-20}$ molecule cm^{-3} for the linear Cl_3, the best fit produces the values $k_{(1a)}=(1.5\pm0.6) \times 10^{-14}$ cm^3 $molecule^{-1}$, $k_{(1b)}=(5.7\pm2.3) \times 10^5$ s^{-1}, $k_{(2)}=(2.5–4) \times 10^{-10}$ cm^3 $molecule^{-1}$ s^{-1}, and $k_d=2500$ s^{-1} as shown in Fig. 2. The decay shapes of Cl_3 were mostly sensitive to $k_{(1a)}$, $k_{(1b)}$, and k_d. Since $k_{(2)}$ was not sensitive, $k_{(2)}$was determined from the pressure dependence as follows. With $K=9.9 \times 10^{-20}$ molecule cm^{-3} for the bent Cl_3, the simulated curve was essentially the same using the kinetic parameters of Table IV.

A simulation with $k_{(1a)}$, $k_{(1b)}$, $k_{(2)}$, and k_d included was performed for the absorption intensity of Cl_3 as a function of Cl_2 concentration. As shown in Fig. 4, the results are essentially the same as approximated by a simple equilibrium Eq.(6).

Figure 5 shows the buffer pressure dependence of the absorption intensity of Cl_3. The production of Cl_3 increased experimentally with total pressure. A model calculation with reactions (1a), (1b), and (2) explains the tendency of this pressure dependence for both linear and bent structures of Cl_3 as shown by the curves in Fig. 5. We used the chemical kinetic simulator software and the rate constants listed in Table IV. Hutton and Wright suggested the upper limit value of $k_{(2)}$ to be 2.8×10^{-10} cm^3 $molecule^{-1}$ s^{-1} at 298 K.[3] Although the experimental data have large error bars, it is safe to say that $k_{(2)}$ is estimated to be in the order of the collisional cross section or $(2.5–4) \times 10^{-10}$ cm^3 $molecule^{-1}$ s^{-1}.

There is another possibility that Cl_3 is formed by the "radical-complex" mechanism that includes the reactions of $Cl+M \rightarrow ClM$ and $ClM+Cl_2 \rightarrow Cl_3+M$. This mechanism is similar to what was suggested by Troe for the OO_2 and ClO_2 formation from corresponding atom and molecule under higher pressure experimental conditions up to 1000 bars.[36] In the present work, we could not confirm the possibility of this radical-complex mechanism under the pressure range up to one quarter of a bar.

TABLE IV. Reactions used for simulations at 213 K and 100 Torr total pressure of N_2 diluent.

Reactions	Rate constant (cm^3 $molecule^{-1}$ s^{-1} or s^{-1})
$Cl+Cl_2+M \rightarrow Cl_3+M$	1.5×10^{-14}
$Cl_3+M \rightarrow Cl+Cl_2+M$	$k_{(1a)}/K$
$Cl+Cl_3 \rightarrow 2Cl_2$	$(2.5-4)\times10^{-10}$
Diffusion	2500

ACKNOWLEDGMENTS

The authors are grateful to Dr. A. J. Orr-Ewing of the University of Bristol for stimulating discussions. One of the authors (S.E.) thanks the JSPS Research Fellowship for Young Scientist.

REFERENCES

[1] D. L. Bunker and N. J. Davidson, J. Am. Chem. Soc. **80**, 5090 (1958).
[2] E. Hutton, Nature (London) **203**, 835 (1964).
[3] E. Hutton and M. Wright, Chem. Soc. Faraday Trans. **61**, 78 (1964).
[4] J. W. Linnett and M. H. Booth, Nature (London) **199**, 1181 (1963).
[5] Y. T. Lee, R. R. LeBreton, J. D. McDonald, and D. R. Hershbach, J. Chem. Phys. **51**, 455 (1969).
[6] M. J. Coggiola, J. J. Valentini, and Y. T. Lee, Int. J. Chem. Kinet. **8**, 605 (1976).
[7] J. J. Valentini, M. J. Cogglia, and Y. T. Lee, Faraday Discuss. Chem. Soc. **62**, 232 (1977).
[8] M. W. Sigrist, D. J. Krajnovich, F. Huisken, Z. J. Zhang, Y. T. Lee, and Y. R. Shen, Helv. Phys. Acta **53**, 289 (1980).
[9] G. Mamantov, D. G. Vickroy, E. J. Vasini, T. Maekawa, and M. C. Moulton, Inorg. Nucl. Chem. Lett. **6**, 701 (1970).
[10] G. Mamantov, E. J. Vasini, M. C. Moulton, D. G. Vickroy, and T. J. Maekawa, Chem. Phys. **54**, 3419 (1971).
[11] M. R. Clarke, W. H. Fletcher, G. Mamantov, E. J. Vasini, and D. G. Vickroy, Inorg. Nucl. Chem. Lett. **8**, 611 (1972).
[12] E. S. Prochaska and L. Andrews, Inorg. Chem. **16**, 339 (1977).
[13] E. S. Prochaska, L. Andrews, N. R. Smyrl, and G. Mamantov, Inorg. Chem. **17**, 970 (1978).
[14] M. Kawasaki, H. Sato, and G. Inoue, J. Phys. Chem. **93**, 7571 (1989).
[15] T. G. Wright, A. J. Bell, and J. G. Frey, Chem. Phys. Lett. **189**, 297 (1992).
[16] W. G. Lawrence, R. M. Fulghum, and M. C. Heaven, J. Phys. Chem. **100**, 18702 (1996).
[17] B. R. De and A. B. Sannigrahi, Int. J. Quantum Chem. **22**, 435 (1982).
[18] E. Vasini and E. J. Castro, J. Mol. Struct. **22**, 415 (1974).
[19] D. L. Thomson, J. Chem. Phys. **60**, 4557 (1974).

[20] J. J. Duggan and R. J. Grice, J. Chem. Soc., Faraday Trans. 2 **80**, 809 (1984).
[21] L. Dalla Riva, S. H. Lin, and H. Eyring, An. Asoc. Quim. Argent. **59**, 133 (1971).
[22] G. L. Gutsev, J. Struct. Chem. **30**, 733 (1989).
[23] A. L. Kaledin, M. C. Heaven, W. G. Lawrence, Q. Cui, J. E. Stevens, and K. Morokuma, J. Chem. Phys. **108**, 2771 (1998).
[24] L. Y. Nelson and G. C. Pimentel, J. Chem. Phys. **47**, 3671 (1967).
[25] C. A. Wight, B. S. Ault, and L. J. Andrew, J. Chem. Phys. **65**, 1244 (1976).
[26] A. O'Keefe and D. A. G. Deacon, Rev. Sci. Instrum. **59**, 2544 (1988).
[27] T. Yu and M. C. Lin, J. Am. Chem. Soc. **115**, 4371 (1993).
[28] M. D. Wheeler, S. M. Newman, A. J. Orr-Ewing, and M. N. R. Ashfold, J. Chem. Soc., Faraday Trans. **94**, 337 (1998).
[29] S. S. Brown, A. R. Ravishankara, and H. Stark, J. Phys. Chem. A **104**, 7044 (2000).
[30] S. Enami, Y. Hoshino, Y. Ito, S. Hashimoto, M. Kawasaki, and T. J. Wallington, J. Phys. Chem. A **110**, 3546 (2006).
[31] K. Suma, Y. Sumiyoshi, Y. Endo, S. Enami, S. Aloisio, S. Hashimoto, M. Kawasaki, S. Nishida, and Y. Matsumi, J. Phys. Chem. A **108**, 8096 (2004).
[32] G. E. Busch, R. T. Mahoney, and R. I. Morse, J. Chem. Phys. **51**, 449 (1969).
[33] M. Kawasaki, K. Suto, Y. Sato, Y. Matsumi, and R. Bersohn, J. Phys. Chem. **100**, 19853 (1996).
[34] S. Baer, H. Hippler, R. Rahn, M. Siefke, N. Seitzinger, and J. Troe, J. Chem. Phys. **95**, 6463 (1991).
[35] M. J. Frisch, G. W. Trucks, H. B. Schlegel *et al.*, GAUSSIAN 03, Revision B.04, Gaussian, Inc., Pittsburgh, PA, 2003.
[36] J. Troe, Chem. Rev. (Washington, D.C.) **103**, 4565 (2003).